Computer simulation studies of the speckle correlations of light scattered from a random array of dielectric spheres of random radii or dielectric constants

B. Danila and A. R. McGurn
Department of Physics, Western Michigan University, Kalamazoo, Michigan 49008-5252, USA
(Received 5 October 2005; revised manuscript received 17 February 2006; published 2 May 2006; publisher error corrected 22 May 2006)

Computer simulation studies are presented for the speckle correlation function for light elastically scattered by a spatially random array of dielectric spheres in three-dimensional space within the context of a scalar wave theory. In addition to the spatial randomness, the spheres in our model are taken to have a statistical distribution of radii and dielectric constants. Results are presented for cases in which the radii of the spheres are much less than the wavelength of the light so that the scattering from the individual spheres is approximately *s*—wave in nature, and the volume filling fraction of the spheres is small. In a first set of simulations a homogeneously random system is considered. A second set of simulations treats a random system that is spatially periodic on average. In both cases, the effects of a statistical distribution of sphere radii and dielectric constants are determined and compared with results presented in Phys. Rev. B **64**, 165204 (2001) for a spatially random array of identical spheres. In a final series of simulations the spheres of the array are taken, in addition to the spatial randomness, to have a Kerr nonlinear dielectric constant. Changes in the speckle correlation functions are determined as a function of the Kerr parameter and incident field intensities. The scalar wave theory has been used recently in the treatment of scattering from random media in which phase interference effects are of interest, e.g., Anderson localization phenomena, speckle correlations, and effects related to universal conductance fluctuations. The scalar field also models acoustical excitations and scalar wave electron propagation in random media.

DOI: 10.1103/PhysRevB.73.174201 PACS number(s): 71.55.Jv, 78.20.Bh, 78.70.−g, 42.25.Dd

I. INTRODUCTION

In this paper computer simulation studies are presented for the speckle correlation functions of the elastic scattering of light by an array of dielectric spheres that are randomly distributed in three-dimensional space.[1] The considerations focus on systems formed from spheres that, in addition, have a statistical distribution of radii or a statistical distribution of dielectric constants or a Kerr nonlinearity. The work represents an extension of that presented in Ref. 1 for the speckle correlation functions of light elastically scattered by a random spatial distribution of identical spheres composed of a single linear dielectric medium. The basis of the studies is a scalar wave treatment.[1–3] This treatment has recently been used to model phase coherent Anderson localization effects, speckle correlations, and universal conductance fluctuations in a variety of optical and other types of physical systems.[4–19] In this regard the scalar wave function can represent effects in randomly disordered optical, acoustical, and electron systems in a polarization-independent format.

The speckle correlation function which provides a quantitative measure of the intensity fluctuations in a speckle pattern is defined by $C(\mathbf{q},\mathbf{k}|\mathbf{q}',\mathbf{k}')=\langle[I(\mathbf{q}|\mathbf{k})-\langle I(\mathbf{q}|\mathbf{k})\rangle][I(\mathbf{q}'|\mathbf{k}')-\langle I(\mathbf{q}'|\mathbf{k}')\rangle]\rangle$, where $I(\mathbf{q}|\mathbf{k})$ is proportional to the differential scattering coefficient for the elastic scattering of light of initial wave vector $\mathbf{k}$ into light of final wave vector $\mathbf{q}$, and $\langle\ \rangle$ denotes an average over a statistical ensemble of random configurations.[1,20–24] It is found to have a number of interesting features that come from the kinematics of the scattering processes, the nature of the interaction of light with a random scattering medium, and the properties of the phase information that are retained by the light as it passes through the medium. As a result the speckle correlation function can be shown to arise from a sum of terms,[5–10,20–23] i.e., $C=C^{(1)}+C^{(10)}+C^{(1.5)}+C^{(2)}+C^{(3)}$, where in this expression the explicit wave vector dependence of C and its terms is given by $C(\mathbf{q},\mathbf{k}|\mathbf{q}',\mathbf{k}')$ and $C^{(i)}(\mathbf{q},\mathbf{k}|\mathbf{q}',\mathbf{k}')$ for $i=1,10,1.5,2,3$. This sum has been studied in a number of works where the terms of the sum have been characterized according to their extent in k space as being short-ranged ($C^{(1)}$ and $C^{(10)}$),[4,5,20,21] long ranged [$C^{(1.5)}$ (Refs. 20 and 21) and $C^{(2)}$ (Ref. 5)], and infinite ranged [$C^{(3)}$ (Ref. 5)]. The strength of their contributions to the correlation function decreases rapidly with increasing range of the correlations so that in the examples treated in this paper only the $C^{(1)}$ and $C^{(10)}$ terms are found in the computer simulation data.[4,5,20,22] The other terms are too weak to be observed to the statistical accuracy of the simulation.[1] The reader can find an excellent review of the general properties of $C^{(1)}$, $C^{(2)}$, and $C^{(3)}$ in Ref. 24 whereas the other terms are discussed in the papers cited earlier. A recent direction of some of this work is in mixed frequency and dynamical correlations as well as in the detailed experimental studies of the properties exhibited by the terms in the sum for C.[6,12,13,25–29]

$C^{(1)}$ occurs in the lowest order of the perturbation expansion of the speckle correlation function in powers of the volume disorder.[4,5,20,21] It has been shown to have important phase coherent peaks in wave vector space, coming from same-path and time-reversed path scattering effects. These arise from different sets of radiation that travel on nearly parallel or nearly antiparallel paths, sampling the same scattering environments. $C^{(10)}$ (Refs. 20 and 21) occurs in the same orders of perturbation theory as $C^{(1)}$ but is distinct from $C^{(1)}$. This difference comes because, as we shall see in the

later discussions, these two contributions to the correlation function sample different regions of the wave vector space for the scattering $\mathbf{k}$ to $\mathbf{q}$ and $\mathbf{k}'$ to $\mathbf{q}'$. As a result, phase coherent processes are not as important in $C^{(10)}$ as they are in $C^{(1)}$.[20,21]

In our simulation, the treatment used to compute these terms is the scalar wave treatment of electromagnetic scattering.[1–3] It has been the basis upon which most of the results cited above for the speckle correlation functions were obtained. It has been shown to present a reasonable representation of some of the general behaviors found in the speckle correlation functions of disordered optical systems, though some difficulties in the treatment will be addressed later and in the conclusions. A comparison of results of the scalar wave treatment of the speckle correlation functions with experiment is discussed in Refs. 6, 12, 13, 15, 16, 24, 27, and 29.

Our interest in systems composed of spheres with a distribution of dielectric constants and radii is to see how these additional types of randomness affect the speckle correlations in a spatially random distribution of spheres, changing them from the speckle correlations in systems with identical spheres. We find that these additional types of randomness can introduce fundamental changes in the speckle correlation functions from those obtained for systems of identical spheres. We also consider the effects of Kerr nonlinearity on a spatially random distribution of identical spheres. In this case the dielectric properties of each sphere depend on the field amplitude applied to the sphere. This amplitude differs from sphere to sphere. We find that for small Kerr interactions, the speckle correlation function of the scattered light in some cases is fundamentally changed from the case of spheres formed from linear dielectric medium. It is interesting, however, that due to the field dependence of the Kerr dielectric, a study of the field dependence of the speckle correlation function can be used to obtain the derivative of the speckle correlation function with respect to the dielectric constant of the spheres.

For our simulation the order of the presentation below is as follows: In Sec. II, the scalar wave treatment is outlined and the form of the speckle correlation function is given. In Sec. III, the model is defined and the equations for a formal exact solution are presented which are later evaluated using computer simulation. An outline of the solution is given in which the reader is referred to Ref. 1 for details. In Sec. IV, the format for the presentation of the speckle correlation function computer simulation data is discussed. In Sec. V, results for systems with random dielectric constants or random radii are presented. In Sec. VI, the results for Kerr nonlinear media are presented. In Sec. VII, the conclusions are presented.

II. SCALAR WAVE TREATMENT AND SPECKLE CORRELATION FUNCTION

Our studies are based on the scalar wave formulation for the scattering of light from the array of spheres.[1–3] In brief outline, the formulation approximates the electromagnetic field as a scalar wave function, $\Psi(\mathbf{r},t)$, satisfying the scalar Helmholtz equation

$$\left(\nabla^2 - \frac{\epsilon(\mathbf{r})}{c^2}\frac{\partial^2}{\partial t^2}\right)\Psi(\mathbf{r},t) = 0, \tag{1}$$

where $\epsilon(\mathbf{r})$ is the position dependent dielectric function. The scattering cross section and speckle correlation function are obtained from Eq. (1) using a computer simulation that generates an essentially exact solution of the scalar field equation for $\Psi(\mathbf{r},t)$ in terms of $\epsilon(\mathbf{r})$. In the scalar formulation the energy current is given by

$$\mathbf{J}(\mathbf{r}) = -\frac{1}{8\pi}\left(\frac{\partial\Psi^*(\mathbf{r},t)}{\partial t}\nabla\Psi(\mathbf{r},t) + \text{c.c.}\right), \tag{2}$$

and the scattering cross section is obtained from the ratio of the outgoing divided by the incoming currents. In this form the scalar wave treatment has been recently applied in many of the speckle correlation function papers cited above. The multiple scattering effects in a disordered media tend to average out polarization effects so that their neglect is less important in randomly disordered systems than in the treatment of the interactions of light with highly symmetric media. For further discussions of the scalar wave formulation and its applications the reader is referred to Refs. 1–3, 16, and 24.

The speckle correlation function we compute measures the angular fluctuations in the scattering cross section.[1,4–11,20–23] It is defined as[1,20–23]

$$C(\mathbf{q},\mathbf{k}|\mathbf{q}',\mathbf{k}') = \left\langle \frac{d\sigma}{d\Omega}(\mathbf{q}|\mathbf{k})\frac{d\sigma}{d\Omega}(\mathbf{q}'|\mathbf{k}')\right\rangle - \left\langle \frac{d\sigma}{d\Omega}(\mathbf{q}|\mathbf{k})\right\rangle\left\langle \frac{d\sigma}{d\Omega}(\mathbf{q}'|\mathbf{k}')\right\rangle, \tag{3}$$

where $(d\sigma/d\Omega)(\mathbf{q}|\mathbf{k})$ is the differential scattering coefficient per sphere for the elastic scattering of light of wave vector $\mathbf{k}$ into light of wave vector $\mathbf{q}$, and $\langle\ \rangle$ denotes an average over the statistical ensemble of the arrays of spheres. Only the most dominant contributions to the speckle correlation function from this sum are treated so that

$$C(\mathbf{q},\mathbf{k}|\mathbf{q}',\mathbf{k}') \approx C^{(1)}(\mathbf{q},\mathbf{k}|\mathbf{q}',\mathbf{k}') + C^{(10)}(\mathbf{q},\mathbf{k}|\mathbf{q}',\mathbf{k}'). \tag{4}$$

In the infinite system (thermodynamic limit), these terms are proportional to $\delta(\mathbf{q}-\mathbf{k}-\mathbf{q}'+\mathbf{k}')$ and $\delta(\mathbf{q}-\mathbf{k}+\mathbf{q}'-\mathbf{k}')$, respectively.

The form of the speckle correlation function defined in Eq. (3) has been of considerable interest recently because it exhibits a number of features that depend on the propagation characteristics or weak localization of electromagnetic waves in the scattering media.[5–10,15–19,25] It also displays features that are analogous to those found in universal conductance fluctuations.[5–8,16,17,19,25] (See, for example, Refs. 14 and 19 for reviews of these topics.)

III. THE MODEL AND THE SIMULATION SOLUTION

The simulation used is for low volume filling fraction arrays of identical spheres with radii small compared to the wavelength of the elastically scattered light.[1] Two types of spatial disorder are treated. In one set of simulations the

spheres have a homogeneously random distribution in space with the restriction that spheres do not overlap. In a second set of simulations the spheres are randomly and uniformly distributed on a periodic lattice. The lattice is taken to be a cubic lattice with a lattice constant equal to the wavelength of the incident light.

The random medium considered consists of a spatially random array of N dielectric spheres.[1] The centers of the spheres are randomly positioned on the vertices of an $m \times m \times m$ simple cubic lattice of lattice constant a, and the faces of the cubic lattice are perpendicular to the x, y, and z axes. For the homogeneously random system the wavelength of the elastically scattered light is taken to be much greater than the lattice constant, while in the periodic on average random system the wavelength of the elastically scattered light is of the order of the lattice constant. Letting $\mathbf{r}_l$, R_l, and ϵ_l denote the center position vector, radius, and dielectric constant of the lth sphere, the electrical permittivity of the medium is written as

$$\epsilon(\mathbf{r}) = 1 + \delta\epsilon(\mathbf{r}), \tag{5}$$

where

$$\delta\epsilon(\mathbf{r}) = \sum_l (\epsilon_l - 1) S_l(\mathbf{r} - \mathbf{r}_l) \tag{6}$$

sums over the array of spheres, and

$$S_l(\mathbf{r}) = \begin{cases} 1 & \text{when } |\mathbf{r}| \leq R_l, \\ 0 & \text{when } |\mathbf{r}| > R_l. \end{cases} \tag{7}$$

The volume fraction of the array of spheres in the cubic lattice is $p = N(4\pi/3)\langle R_i^3 \rangle / (ma)^3$. The derivation of the formal scattering solution for the system that is the basis of our simulation was given in Ref. 1. Below we shall indicate the changes in it in the presence of the new types of disorder.

For the system of spheres in Eqs. (5)–(7), Eq. (16) in Ref. 1 for the scattered wave from the array of scatterers becomes

$$\psi_{sc}(\mathbf{r}) = \frac{3}{4\pi}\left(\frac{\omega}{c}\right)^2 \frac{e^{ik_0 r}}{r} \sum_{k,l} e^{-ik_0 \hat{r}\cdot\mathbf{r}_k} (\epsilon_k - 1) V_k \frac{j_1(k_0 R_k)}{k_0 R_k} \times \left[\tilde{1} - \tilde{M} \frac{\tilde{\epsilon} - 1}{4\pi} \left(\frac{\omega}{c}\right)^2 \right]^{-1}_{\mathbf{r}_k, \mathbf{r}_l} \psi_{inc}(\mathbf{r}_l). \tag{8}$$

Here k and l label quantities referring to the kth and lth spheres in the array, $\tilde{\epsilon} = \epsilon_i \delta_{i,j}$, $k_0 = \omega/c$, V_k is the volume of the kth particle, $j_1(x)$ is the spherical Bessel function of order 1, and $\psi_{inc}(\mathbf{r})$ is the incident wave. The matrix $\tilde{M}$ is defined in Eq. (17) of Ref. 1 where it is shown that its elements are given by $M_{\mathbf{r}_k, \mathbf{r}_l} = \int_{V_l} d^3u\, G[\mathbf{r}_k | \mathbf{r}_l + \mathbf{u}]$ for the Green's function $G[\mathbf{r}|\mathbf{r}'] = \exp[i(\omega/c)|\mathbf{r} - \mathbf{r}'|]/|\mathbf{r} - \mathbf{r}'|$. The scattering cross section per sphere in the far-field limit is

$$\frac{d\sigma}{d\Omega}(\mathbf{q}|\mathbf{k}) = |f(\hat{q}, \hat{k})|^2 / N, \tag{9}$$

where the scattering amplitude of the array, $f(\hat{q}, \hat{k})$, is the coefficient of $e^{ik_0 r}/r$ in Eq. (8). [Note: The results in Eqs. (8) and (9) and Eq. (16) of Ref. 1 are examples of the **T**-matrix formulation of scattering, treating all the multiple scattering from and between the spheres of our model. Examples of the **T**-matrix formulation and its derivation in the context of quantum mechanics can be found in Refs. 30–32. The derivation in Ref. 1 essentially parallels these treatments within the context of our model.]

IV. PRESENTATION OF THE SPECKLE CORRELATION FUNCTION DATA

In the thermodynamic limit the condition for nonzero $C^{(1)}(\mathbf{q}, \mathbf{k} | \mathbf{q}', \mathbf{k}')$ is $\mathbf{q} - \mathbf{k} - \mathbf{q}' + \mathbf{k}' = 0$, while the condition for nonzero $C^{(10)}(\mathbf{q}, \mathbf{k} | \mathbf{q}', \mathbf{k}')$ is $\mathbf{q} - \mathbf{k} + \mathbf{q}' - \mathbf{k}' = 0$. Consequently, in this paper scans are presented of the $C^{(1)}(\mathbf{q}, \mathbf{k} | \mathbf{q}', \mathbf{k}')$ and $C^{(10)}(\mathbf{q}, \mathbf{k} | \mathbf{q}', \mathbf{k}')$ nonzero envelopes. These contributions dominate the topography of the correlation functions and are obtained when $(\mathbf{q}, \mathbf{k}, \mathbf{q}', \mathbf{k}')$ are varied such that either $\mathbf{q} - \mathbf{k} - \mathbf{q}' + \mathbf{k}' = 0$ or $\mathbf{q} - \mathbf{k} + \mathbf{q}' - \mathbf{k}' = 0$ are always satisfied.

For $C^{(1)}(\mathbf{q}, \mathbf{k} | \mathbf{q}', \mathbf{k}')$, the envelope condition means that $(\mathbf{q} - \mathbf{k})$ and $(\mathbf{q}' - \mathbf{k}')$ are parallel vectors of the same magnitude. A convenient parametrization of the envelope is obtained by choosing[1]

$$\mathbf{k} = k_0(\sin\theta, 0, \cos\theta), \quad \mathbf{k}' = k_0(\sin\theta, 0, -\cos\theta),$$

$$\mathbf{q} = k_0(\sin\theta\cos\phi, \sin\theta\sin\phi, \cos\theta),$$

$$\mathbf{q}' = k_0(\sin\theta\cos\phi, \sin\theta\sin\phi, -\cos\theta), \tag{10}$$

where $0° \leq \theta \leq 180°$ and $0° \leq \phi \leq 360°$. Since the correlation function is symmetric under reflection through the x-y plane, the angle θ need only run from 0° to 90°. There is also symmetry of the correlation function under reflection in the x-z plane so that ϕ can be restricted to run from 0° to 180°. In the following, scans of the $C^{(1)}$ envelope are made in θ at constant azimuthal angles $\phi = 0°$ and 90°. For the case in which $\phi = 0°$ the vectors $\mathbf{k}$ and $\mathbf{q}$ are parallel and when reflected in the x-y plane give the parallel vectors $\mathbf{k}'$ and $\mathbf{q}'$. For the case in which $\phi = 90°$ the vectors $\mathbf{k}$ and $\mathbf{q}$ are mapped into each other when $\mathbf{k}$ is rotated 90° counter-clockwise in the x-y plane. The vectors $\mathbf{k}'$ and $\mathbf{q}'$ are obtained from $\mathbf{k}$ and $\mathbf{q}$, respectively, by reflecting $\mathbf{k}$ and $\mathbf{q}$ in the x-y plane. The plane of incidence (containing $\mathbf{k}$, $\mathbf{k}'$) then intersects the scattering plane (containing $\mathbf{q}$, $\mathbf{q}'$) at right angles.

The envelope condition for $C^{(10)}(\mathbf{q}, \mathbf{k} | \mathbf{q}', \mathbf{k}')$ means that $(\mathbf{q} - \mathbf{k})$ and $(\mathbf{q}' - \mathbf{k}')$ must be antiparallel vectors of the same magnitude. This condition can be fulfilled when[1]

$$\mathbf{k} = k_0(\sin\theta, 0, \cos\theta), \quad \mathbf{k}' = k_0(-\sin\theta, 0, \cos\theta),$$

$$\mathbf{q} = k_0(\sin\theta\cos\phi, \sin\theta\sin\phi, \cos\theta),$$

$$\mathbf{q}' = k_0(-\sin\theta\cos\phi, -\sin\theta\sin\phi, \cos\theta). \tag{11}$$

Again, due to symmetry considerations, plots are presented for $0° \leq \theta \leq 90°$ and only results for the constant azimuthal angles $\phi = 0°$ and 90° are given. The $\phi = 0°$ results are for parallel $\mathbf{k}$ and $\mathbf{q}$, which when reflected in the y-z plane give $\mathbf{k}'$ and $\mathbf{q}'$, respectively. In the $\phi = 90°$ results, the x-z plane containing $\mathbf{k}$ and $\mathbf{k}'$ is at a right angle to the y-z plane containing $\mathbf{q}$ and $\mathbf{q}'$.

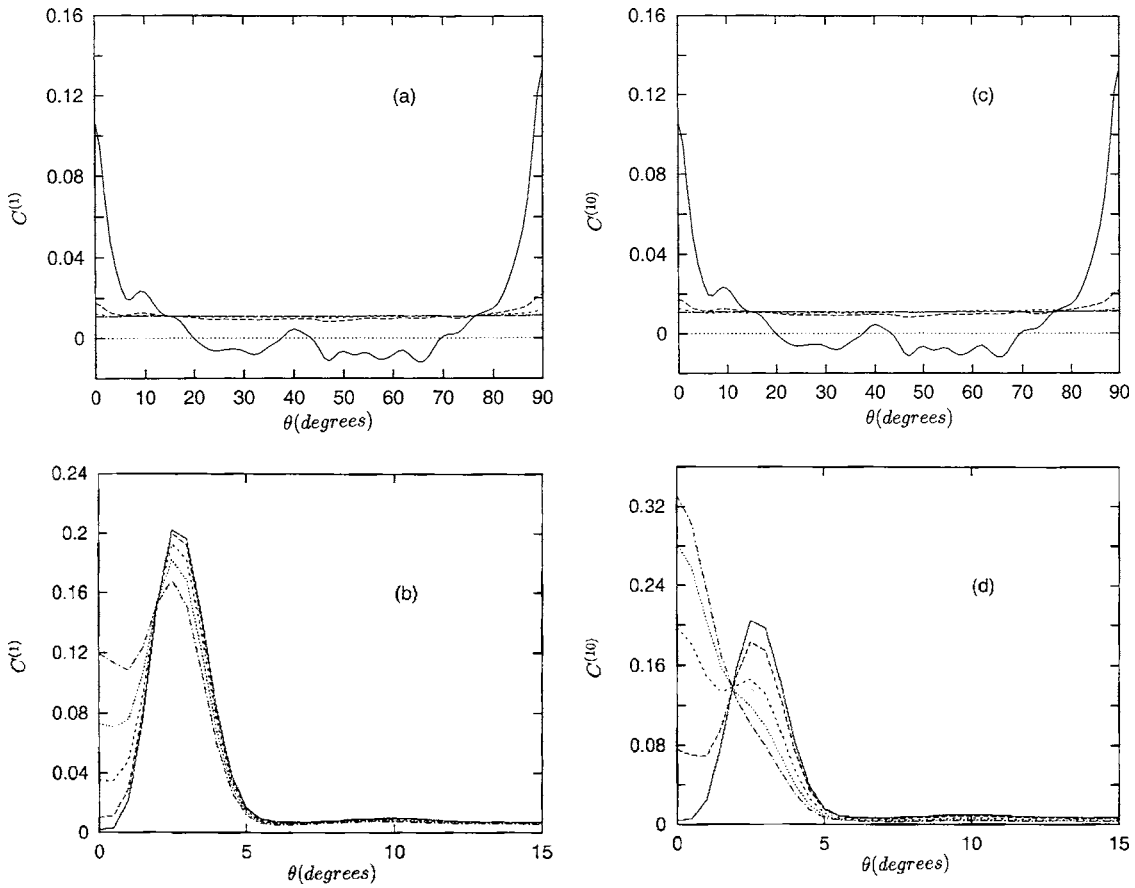

FIG. 1. Plots for the $\epsilon=-5$ homogeneously random system of the angular speckle correlation function along the $C^{(1)}$ envelope, scanned as a function of θ for (a) $\phi=0°$ and (b) $\phi=90°$. On the left-hand side of (a) the curves are from top to bottom: $\sigma_\epsilon=0$, 0.25, 0.5, 1.0, 1.5, and 2.0. The results for $\sigma_\epsilon=0.5$, 1.0, 1.5, and 2.0 are indistinguishable on the plot and appear as flat lines. In (b) curves are presented over the restricted range $0° \leqslant \theta \leqslant 15°$ for $\sigma_\epsilon=0$, 0.5, 1.0, 1.5, and 2.0 (bottom to top on the left-hand edge of the plot). In (b) at $\theta=0°$ the curves are increasing functions of σ_ϵ and are essentially flat and indistinguishable in the region $5° \leqslant \theta \leqslant 90°$. For comparison, results are also presented of the $\epsilon=-5C^{(10)}$ envelope as a function of θ for (c) $\phi=0°$ with $\sigma_\epsilon=0$,0.25,0.5,1.0,1.5,2.0, top to bottom on the left-hand edge, and (d) $\phi=90°$ with $\sigma_\epsilon=0$,0.5,1.0,1.5,2.0, bottom to top on the left-hand edge.

To simulate the homogeneously random system the wavelength of light is chosen such that $\lambda/a=8$, and to simulate the periodic on average system $\lambda/a=1$. This assures that in the former case the periodic lattice is not important and the system appears homogeneous to the incident light whereas it is an essential part of the physics in the latter case. The average volume of the spheres in the array is chosen with $4\pi\langle R^3\rangle/3\lambda^3=1.0808\times10^{-3}$ where R is the radius of a sphere so that $4\pi\langle R^3\rangle/3a^3=5.534\times10^{-1}$ for the homogeneous system and $4\pi\langle R^3\rangle/3a^3=1.0808\times10^{-3}$ for the periodic on average system. The volume filling fraction of the runs is fixed by choosing m and N to give $p=1.855\times10^{-4}$ for the homogeneous system and $p=1.827\times10^{-4}$ for the periodic on average system. The simulation results are generated from samplings of 500 and 1000 randomly generated configurations with results presented for average dielectric constants $\epsilon=-5$, -2, 0, 2, and 5.

V. RESULTS FOR A DISTRIBUTION OF DIELECTRIC CONSTANTS OR RADII

We first discuss systems in which the spheres have identical radii and the dielectric constants of the spheres are Gaussianly distributed about a mean value $\langle\epsilon\rangle$ with a variance $\sigma_\epsilon^2=\langle(\epsilon-\langle\epsilon\rangle)^2\rangle$. The correlation functions are studied as functions of σ_ϵ. This is followed by a discussion of systems of spheres with identical dielectric constants and with a Gaussian distribution of radii.

A. Distribution of dielectric constants

Consider systems in which the radii of the spheres are fixed and the dielectric constants of the spheres are Gaussianly distributed about a mean value. Runs on the homogeneously random system are made with $m=71$ and $N=120$ and runs on the periodic on average system are made with $m=11$ and $N=225$. The radii of the spheres are fixed at $2\pi R/\lambda=0.4$ and results are presented for $\sigma_\epsilon=0$, 0.5, 1.0, 1.5, and 2.0.

1. Homogeneously random spatial distributions

In Fig. 1 the results are for the homogeneous system. Figures 1(a) and 1(b) show $C^{(1)}(\mathbf{q},\mathbf{k}|\mathbf{q}',\mathbf{k}')$ for average $\epsilon=-5$ systems at $\phi=0°$ and $\phi=90°$, respectively. (Note: To simplify the notation, in systems with random dielectric con-

stants we shall take $\epsilon=\langle\epsilon\rangle$ unless otherwise specified.) These are plotted as functions of θ with the curves labeled by σ_ϵ. In the plots the integrated area under each curve for $0^\circ \leqslant \theta \leqslant 90^\circ$ has been normalized to unity. Two peaks are observed at $\theta=0^\circ$ and 90° in $C^{(1)}$ as a function of θ for the $\sigma_\epsilon=0.0$, $\phi=0^\circ$ data. These were a focus of the discussions for $\sigma_\epsilon=0$ given in Ref. 1 and are seen to disappear with increasing σ_ϵ, being no longer present at $\sigma_\epsilon=0.5$. In the results of Fig. 1(b) for $\phi=90^\circ$ a peak for $\theta<5^\circ$ is observed in the $\sigma_\epsilon=0$, 0.5, 1.0, 1.5, and 2.0 results. For $5^\circ<\theta\leqslant 90^\circ$ all of the $\phi=90^\circ$ curves of $C^{(1)}$ are essentially flat so that only results for $0^\circ \leqslant \theta \leqslant 15^\circ$ are shown in Fig. 1(b). The $\sigma_\epsilon=0$ peak in Fig. 1(b) was a focus of the discussions in Ref. 1. It is seen, as with the peaks in Fig. 1(a), to decrease with increasing dielectric disorder in the system. In the following we review the origins of these features as discussed in Ref. 1 and then indicate how they are suppressed with the introduction of dielectric randomness into our system.

The details of the origin of the features in the $\sigma_\epsilon=0$ data in Figs. 1(a) and 1(b) have been discussed in Ref. 1. Here we just note that, in Fig. 1(a), near $\theta=90^\circ$ and 0° same-path and time-reversed path scattering sequences, respectively, lead to small enhancements in the speckle correlation function. What is meant by this is that at $\theta=90^\circ$ the intermediary processes in the $\mathbf{k}\rightarrow\mathbf{q}$ and $\mathbf{k}'\rightarrow\mathbf{q}'$ scattering from the random media have components that travel along closely parallel paths, sampling the same media. These are same-path sequences and they allow the light in the different scatterings to retain phase coherence. The scattering along these paths gives a correlated contribution to the average

$$\left\langle \frac{d\sigma(\mathbf{q}|\mathbf{k})}{d\Omega}\frac{d\sigma(\mathbf{q}'|\mathbf{k}')}{d\Omega}\right\rangle$$

but only contributes an uncorrelated contribution to the

$$\left\langle \frac{d\sigma(\mathbf{q}|\mathbf{k})}{d\Omega}\right\rangle\left\langle \frac{d\sigma(\mathbf{q}'|\mathbf{k}')}{d\Omega}\right\rangle.$$

This is the origin of the enhancement in the speckle correlation function. A similar situation is found at $\theta=0^\circ$ where the light for $\mathbf{k}\rightarrow\mathbf{q}$ and $\mathbf{k}'\rightarrow\mathbf{q}'$ scattering has components that move along closely parallel paths but in opposite directions. These are time-reversed path sequences (sampling similar regions of the media) that again maintain a phase coherence between the two scatterings. The phase coherence contributes differently to the two averages discussed above. Upon the introduction of the new component of dielectric disorder into the system, the additional fluctuations contribute to the scattering at all angles, rapidly increasing the speckle correlation function at general angles. These contributions quickly overwhelm the phase coherent contributions at $\theta=0^\circ$ and 90°.

In the results in Fig. 1(b) the plane containing both incident wave vectors is at right angles to the plane containing both of the outgoing wave vectors. Consequently, the scattering in a different region of k space is being correlated from that treated in Fig. 1(a). Near $\theta=0^\circ$ in Fig. 1(b) time-reversed paths are contributing to the enhancement. These contributions are again seen to decrease with the introduction of the new disorder. At $\theta=0^\circ$ itself the $\phi=0^\circ$ and $\phi=90^\circ$ branches of the correlation function merge. At the $\theta=0^\circ$ merge point in Fig. 1(b) a peak develops with increasing disorder. This peak comes from the symmetry differences of the $\phi=0^\circ$ and $\phi=90^\circ$ scans, i.e., for $\phi=0^\circ$ the planes containing the incident and scattered wave vector are parallel while for $\phi=90^\circ$ these planes are at right angles. This causes the rate of increase of the angle-independent contributions to the speckle correlation function with disorder to differ between the $\phi=0^\circ$ and 90° data.

The general features in the $\epsilon=-5$ data (i.e., peaks and regions of angular independence) are also found in the data for $\epsilon=-2,0,2,5$ studied as functions of σ_ϵ. The conditions for the disappearance of the enhancements in the correlation functions are also roughly independent of ϵ. Instead of presenting a large collection of graphs generated on these systems and to facilitate a comparison between the correlation functions with different Gaussian dielectric distributions, it is best to consider the results for the unnormalized $C^{(1)}$ integrated over θ. This gives a good idea of how the general features of $C^{(1)}$ depend on ϵ and σ_ϵ and shows how the θ-integrated data for $C^{(1)}$ can be used to distinguish between systems with different ϵ and σ_ϵ.

The area under the curves of $C^{(1)}$ versus θ (i.e., in the unnormalized data) is computed as a function of σ_ϵ for each ϵ. Using linear regression the integrated data are fitted by the form

$$A(\epsilon,\sigma_\epsilon)=A_0(\epsilon)+S(\epsilon)\sigma_\epsilon^\gamma. \tag{12}$$

Here $A(\epsilon,\sigma_\epsilon)$ is the area under the unnormalized curve, $A_0(\epsilon)=A(\epsilon,\sigma_\epsilon=0)$, and $S(\epsilon)$ and $\gamma(\epsilon)$ are fitting parameters determined for each of the ϵ data. Equation (12) gives a general idea of the increasing strengths of the speckle correlations with increasing disorder. In addition, it gives important statistical properties of the dependence of the speckle correlation functions on the disorder. The form in Eq. (12) is from the scaling theory of condensed matter and statistical physics, and we expect from general principles for it to be valid for our system. A central focus will be the determination of the critical exponent, γ, and its universality properties. The reader is referred to the Appendix for more details regarding scaling, critical exponents, the idea of universality, and the application of these ideas to the speckle correlation function.

Results for the exponent $\gamma(\epsilon)$ plotted versus ϵ are shown in Fig. 2(a) for both $\phi=0^\circ$ and $\phi=90^\circ$ data. The dependence of $\gamma(\epsilon)$ on ϵ is found to be quite similar in both $\phi=0^\circ$ and $\phi=90^\circ$ plots. In general $\gamma(\epsilon)$ is slightly greater for $\epsilon>0$ than for $\epsilon<0$ but is otherwise relatively independent of ϵ. This indicates that γ deviates only weakly from universality with respect to ϵ.

The $\phi=0^\circ$ and $\phi=90^\circ$ values of $\ln S(\epsilon)$ and the integrated area, $A_0(\epsilon)$, under the $\sigma_\epsilon=0$ curves are presented in Tables I and II, respectively. For comparison, in Table II the ratio of $A_0(\epsilon)$ computed at $\phi=0^\circ$ divided into $A_0(\epsilon)$ computed at $\phi=90^\circ$ is given. It is interesting to note from this ratio that $A_0(\epsilon)$ at these two different angles exhibits quite different behaviors as functions of ϵ. This is also true of $\ln S$ as a

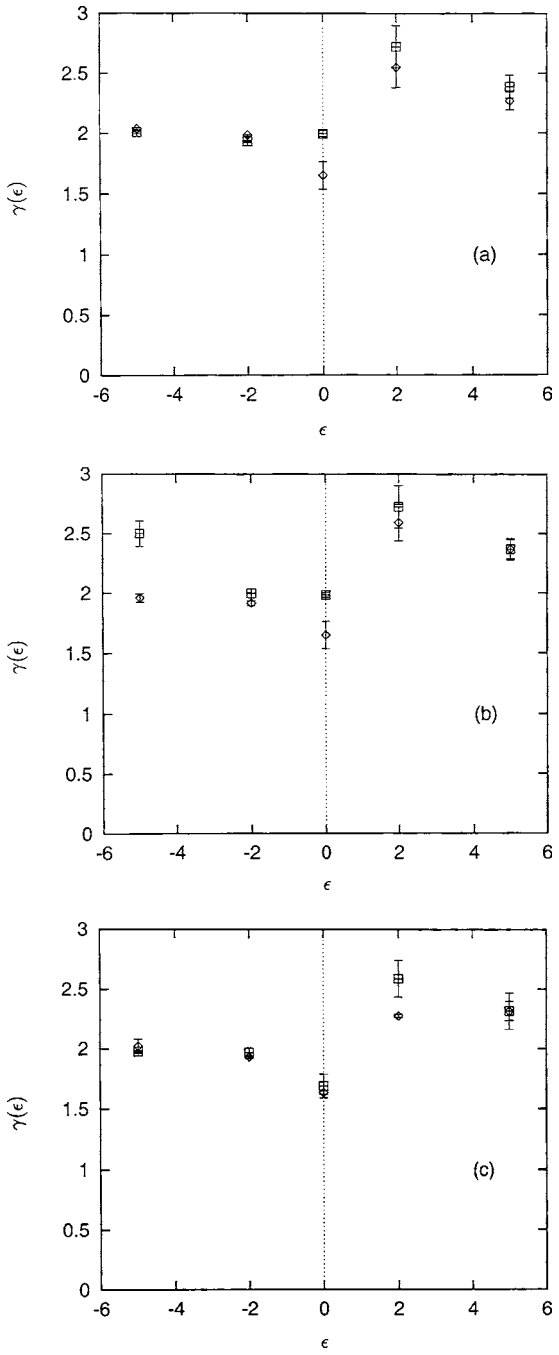

FIG. 2. A plot of $\gamma(\epsilon)$ versus ϵ is given for both $\phi=0°$ (diamonds) and 90° (squares) for the (a) homogeneous system for $C^{(1)}$, (b) homogeneous system for $C^{(10)}$, and (c) periodic on average systems for $C^{(1)}$ composed of spheres with dielectric constants that are statistically distributed about the average value ϵ.

function of ϵ between the two different ϕ, and $\ln S$ is also seen to be strongly dependent on ϵ for both angles. These properties strongly mark the dielectric properties of the scattering system. In this regard it is noted in general that the addition of dielectric randomness in ϵ quickly increases the diffuse scattering and the speckle correlation functions in our system. The reason for this is that our system was originally chosen to have weak scattering so that same-path and time-reversed path enhancement could be observed.

TABLE I. Random dielectric constant parameters $\ln S(\epsilon)$ and $A_0(\epsilon)$ for $\phi=0°$.

Type	ϵ	$\ln S$	A_0
homogeneous $C^{(1)}$	−5	−3.56±0.01	1.600×10^{-4}
homogeneous $C^{(1)}$	−2	−3.91±0.01	6.979×10^{-6}
homogeneous $C^{(1)}$	0	−5.496±0.06	2.700×10^{-8}
homogeneous $C^{(1)}$	2	−3.93±0.09	5.219×10^{-8}
homogeneous $C^{(1)}$	5	0.27±0.04	1.124×10^{-3}
periodic $C^{(1)}$	−5	−2.92±0.03	2.044×10^{-3}
periodic $C^{(1)}$	−2	−3.28±0.05	9.482×10^{-5}
periodic $C^{(1)}$	0	−4.79±0.08	3.042×10^{-7}
periodic $C^{(1)}$	2	−3.37±0.06	8.158×10^{-7}
periodic $C^{(1)}$	5	1.04±0.07	1.858×10^{-2}
homogeneous $C^{(10)}$	−5	−3.52±0.02	1.600×10^{-4}
homogeneous $C^{(10)}$	−2	−3.88±0.01	6.979×10^{-6}
homogeneous $C^{(10)}$	0	−5.50±0.06	2.112×10^{-8}
homogeneous $C^{(10)}$	2	−3.96±0.08	5.219×10^{-8}
homogeneous $C^{(10)}$	5	0.31±0.05	1.124×10^{-3}

An equally important contribution in the speckle correlation function to that of $C^{(1)}$ is the $C^{(10)}$ contribution. In Figs. 1(c) and 1(d) results for $C^{(10)}$ versus θ with $\epsilon=-5$ are shown for $\phi=0°$ and $\phi=90°$, respectively. The data are for systems of spheres randomly and homogeneously distributed in space with the same distributions used in generating the data presented in Figs. 1(a) and 1(b). As in Figs. 1(a) and 1(b) the areas under the $0° \leqslant \theta \leqslant 90°$ curves are normalized to unity. The results at $\phi=0°$ for $C^{(1)}$ and $C^{(10)}$ are very similar. However, the $\phi=90°$ results for $C^{(1)}$ and $C^{(10)}$ exhibit small quantitative differences near $\theta=0°$ as σ_ϵ is increased. These differences could be useful in determining the statistical disorder of the system of spheres from measurements of the correlation functions.

TABLE II. Random dielectric constant parameters $\ln S(\epsilon)$ and $A_0(\epsilon,\phi=90°)/A_0(\epsilon,\phi=0°)$ for $\phi=90°$.

Type	ϵ	$\ln S$	$A_0(\phi=90°)/A_0(\phi=0°)$
homogeneous $C^{(1)}$	−5	−7.48±0.01	52.57
homogeneous $C^{(1)}$	−2	−7.63±0.01	150.30
homogeneous $C^{(1)}$	0	−9.00±0.01	832.56
homogeneous $C^{(1)}$	2	−7.48±0.09	803.46
homogeneous $C^{(1)}$	5	−3.19±0.05	29.39
periodic $C^{(1)}$	−5	−4.82±0.01	11.50
periodic $C^{(1)}$	−2	−5.13±0.01	31.64
periodic $C^{(1)}$	0	−6.66±0.05	215.40
periodic $C^{(1)}$	2	−5.11±0.08	155.19
periodic $C^{(1)}$	5	−0.78±0.04	6.09
homogeneous $C^{(10)}$	−5	−7.78±0.06	52.51
homogeneous $C^{(10)}$	−2	−7.68±0.01	157.62
homogeneous $C^{(10)}$	0	−9.00±0.01	1064.73
homogeneous $C^{(10)}$	2	−7.48±0.19	802.88
homogeneous $C^{(10)}$	5	−3.23±0.04	29.18

TABLE III. Random radii parameters $\ln S(\epsilon)$ and $A_0(\epsilon)$ for $\phi=0°$.

Type	ϵ	$\ln S$	A_0
homogeneous $C^{(1)}$	−5	1.42±0.27	1.600×10^{-4}
homogeneous $C^{(1)}$	−2	−0.28±0.27	6.979×10^{-6}
homogeneous $C^{(1)}$	0	−3.62±0.19	2.112×10^{-8}
homogeneous $C^{(1)}$	2	−2.10±0.01	5.219×10^{-8}
homogeneous $C^{(1)}$	5	4.91±0.25	1.124×10^{-3}

A discussion of the enhancements in Fig. 1(c) at $\theta=0°$ and 90° in the $\sigma_\epsilon=0$ data was given in Ref. 1. At $\theta=0°$ the correlation is between scattering processes containing components composed of same-path sequences. These give rise to enhancements by the same mechanisms as discussed above for the contributions of these processes to the $C^{(1)}$ term. At $\theta=90°$ time-reversed sequences are involved, and our earlier discussions regarding these types of processes apply. The phase coherent enhancements are [as was found in Fig. 1(a)] observed to be overwhelmed by the rapid increase in the general angle diffuse scattering effects on the correlation function as the media fluctuations increase. A discussion of the enhancement at $\theta=0°$ in Fig. 1(d) was given in Ref. 1. In this system the enhancement is related to same-path sequences near $\theta=0°$ and to the merging of the $\phi=0°$ with the $\phi=90°$ correlation functions at $\theta=0°$. The arguments for the changes in the $C^{(10)}$ correlation function presented in Figs. 1(d) upon increasing disorder are the same as given earlier for the results in Fig. 1(b).

In Tables I and II results from a linear regression fit of Eq. (12) to the unnormalized θ-integrated data for $C^{(10)}$ are presented. This is done as the same general features (i.e., peaks and regions of angular independence) of $C^{(10)}$ in Figs. 1(c) and 1(d) are found as ϵ is changed. The results for $\ln S(\epsilon)$ and $A_0(\epsilon)$ in Tables I and II for the $C^{(1)}$ and $C^{(10)}$ systems are similar in spite of the differences in the plots in Figs. 1(b) and 1(d). Our general remarks regarding $\ln S$ and $A_0(\epsilon)$ are the same for both $C^{(1)}$ and $C^{(10)}$. The exponents $\gamma(\epsilon)$ for the $C^{(10)}$ systems are shown in Fig. 2(b). The dependence of $\gamma(\epsilon)$ on ϵ exhibits similar features in $C^{(1)}$ and $C^{(10)}$. In particular, the results for $\gamma(\epsilon)$ are weakly dependent on ϵ and display a behavior that is roughly universal.

2. Periodic on average spatial distributions

In Fig. 3 results on the periodic on average systems for $C^{(1)}$ versus θ are presented for $\epsilon=-5$ at $\phi=0°$ and 90°. The presentation in Fig. 3(a) of the $\phi=0°$ results is similar to that given in Fig. 1(a) for $C^{(1)}$ at $\phi=0°$ for the homogeneously random systems. In the periodic on average system four peaks are observed as a function of θ in the $\sigma_\epsilon=0.0$ data for $C^{(1)}$. These arise from phase coherent effects discussed later. Figures 3(b) and 3(c) are for $C^{(1)}$ [normalized as in Fig. 1(b)] at $\phi=90°$ for $0°\leqslant\theta\leqslant15°$ and $60°\leqslant\theta\leqslant90°$. In the region $15°\leqslant\theta\leqslant60°$, $C^{(1)}$ at $\phi=90°$, aside from a small peak at 30°, is flat and featureless. The peaks observed in the $\phi=90°$ data are associated again with phase coherent processes.

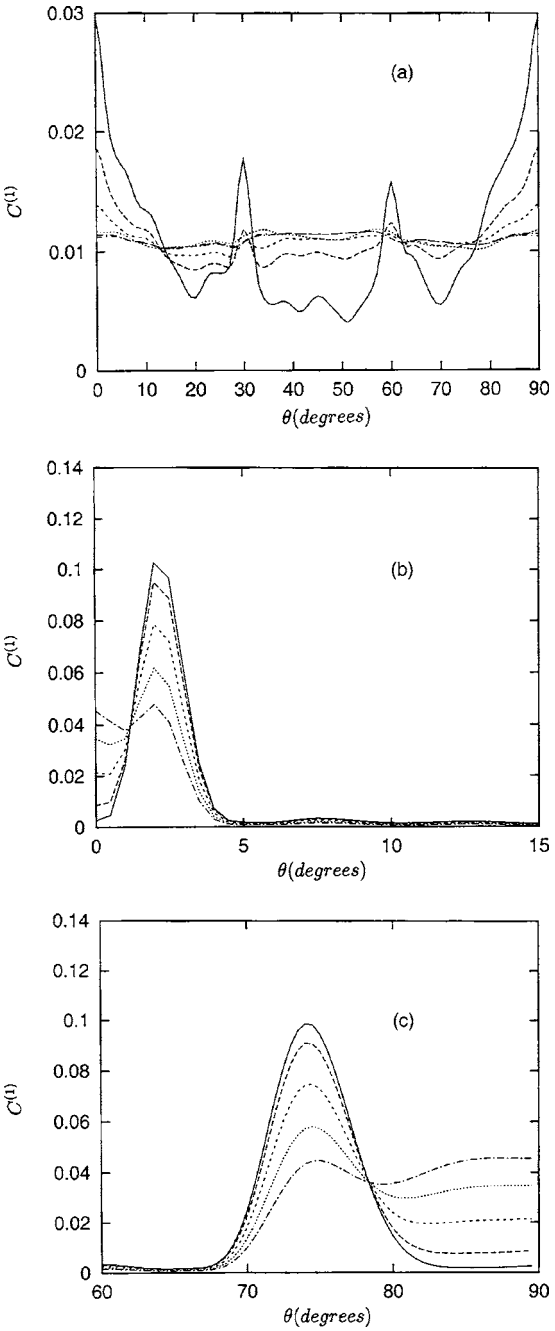

FIG. 3. Plots of the angular speckle correlation function along the $C^{(1)}$ envelope for the periodic on average system with $\epsilon=-5$, scanned as a function of θ for (a) $\phi=0°$, (b) $\phi=90°$ for $0°\leqslant\theta\leqslant15°$, and (c) $\phi=90°$ for $60°\leqslant\theta\leqslant90°$. The curves in (a) are normalized in the same way as are the curves in Fig. 1(a) and the curves in (b) and (c) are normalized in the same way as are those curves in Fig. 1(b). In (a) curves are presented for $\sigma_\epsilon=0.0$, 0.25, 0.5, 1.0, 1.5, and 2.0. As σ_ϵ is increased the curves flatten. In (b) and (c) curves are presented for $\sigma_\epsilon=0$, 0.5, 1.0, 1.5, and 2.0. In (b) [(c)] at $\theta=0°$ (90°), the curves are increasing functions of σ_ϵ.

The phase coherent peaks in Fig. 3 are related to a remnant of Bragg scattering in the periodic on average system, i.e., at the conditions for $\mathbf{k}$ or $\mathbf{k}'$ to undergo Bragg scattering. They are manifest in an increase in the speckle correlation functions near the Bragg scattering angles. As discussed in

Ref. 1 for the $\sigma_\epsilon=0$ limit, the periodic on average disordered system preferentially directs the scattering along paths near the Bragg conditions. These phase coherent processes give an enhancement to the speckle correlation function because of the different way in which they contribute to

$$\left\langle \frac{d\sigma(\mathbf{k}|\mathbf{q})}{d\Omega}\frac{d\sigma(\mathbf{k}'|\mathbf{q}')}{d\Omega} \right\rangle$$

and

$$\left\langle \frac{d\sigma(\mathbf{k}|\mathbf{q})}{d\Omega} \right\rangle \left\langle \frac{d\sigma(\mathbf{k}'|\mathbf{q}')}{d\Omega} \right\rangle.$$

In the first average the phase coherence in the two similar scattering processes is retained in the average whereas in the second average the two similar phase coherent scattering processes contribute to an uncorrelated average. With the increase in dielectric disorder, the isotropic component of scattering increases rapidly and the speckle correlation functions rapidly increase at general angles so as to swamp the phase coherent features.

A series of $\epsilon=-5,-2,0,2,5$ systems were studied for the periodic system, showing the same rates of decrease of the phase coherent enhancements. The plots exhibit the same general features of peaks and angular independent regions as the data presented in Fig. 3, and only a comparison of the various unnormalized $C^{(1)}$ and $C^{(10)}$ data integrated over θ is made. Equation (12) is used again to fit data for the periodic on average system. Figure 2(c) presents results for $\gamma(\epsilon)$ versus ϵ from such a fit of the $C^{(1)}$ data from the periodic on average systems. In Tables I and II results from the periodic on average systems are presented for $\ln S(\epsilon)$ and $A_0(\epsilon)$ from fits of Eq. (12) to all the ϵ simulation data for $C^{(1)}$.

The data in Fig. 2 and Tables I and II indicate that there is a similar dependence on the dielectric constant for the data generated from the homogeneous and the periodic on average systems. Regions of increase or decrease of $A_0(\epsilon)$, $\ln S$, and $\gamma(\epsilon)$ on increasing ϵ seem to correlate between the sets of homogeneous and periodic on average data for the same $\phi=0°$ and 90°. (It is important to note, however, that the absolute values in these data can be quite different.) This is the case even though geometrically the functional dependence of $C^{(1)}$ and $C^{(10)}$ on θ can be quite different in the homogeneous and periodic on average systems. The critical exponent γ again displays a mild dependence on ϵ, but does not appear to depend on whether the system has homogeneous or periodic on average disorder.

B. Distribution of radii

We consider spatially random systems of spheres composed of identical dielectric media. In addition to the randomness in the location of spheres in space, the radii of the spheres are also given a statistical distribution. The radii of the spheres in the array are Gaussianly distributed about an average radius $\langle R\rangle$ with a variance $\sigma_R^2=\langle(R-\langle R\rangle)^2\rangle$. An additional constraint is placed on the distribution that the radii of the spheres must be positive so that when a negative radius is generated in the simulation it is removed from the distribution. This has a small effect on the large σ_R cases treated in our studies. To facilitate a comparison between systems with different statistical distributions of radii, the $\langle R\rangle$ and σ_R are chosen such that $\langle R^3\rangle=\langle R\rangle^3+3\langle R\rangle\sigma_R^2$ is fixed. This maintains a constant volume filling fraction of the random array of spheres in space for both homogeneous and periodic on average systems. Simulation data generated in this way are studied as functions of ϵ, $\langle R\rangle$, and σ_R for fixed spatial filling fraction.

In Fig. 4 $C^{(1)}$ versus θ is presented for the homogeneous and periodic on average systems with $\epsilon=-5$. The definitions of the homogeneous and periodic on average systems are the same as used in generating the data presented in Figs. 1 and 3. Results are shown in Figs. 4(a) and 4(b) for the homogeneous random system for $\phi=0°$ and 90°, respectively. As in Fig. 1 the plots are normalized so that the area under each curve is unity over $0°\leqslant\theta\leqslant 90°$ for both $\phi=0°$ and $\phi=90°$. The $\phi=0°$ data in Fig. 4(a) are shown for $\sigma_R/\langle R\rangle=0.0$, 0.01, 0.05, 0.1, 0.25, and 0.5 corresponding to $2\pi\langle R\rangle/\lambda=0.4$, 0.399 96, 0.399 00, 0.396 08, 0.377 73, and 0.331 93, respectively. For $0.05<\sigma_R/\langle R\rangle$ the peaked features in the data near $\theta=0°$ and 90° disappear so that the curves for $C^{(1)}$ are essentially flat over $0°\leqslant\theta\leqslant 90°$. The origin of these peaks are from same-path ($\theta=90°$) and time-reversed path ($\theta=0°$) scatterings, and the disappearance of the enhancements is due to the swamping of the phase coherent contributions by the increased general scattering in the system. In this regard, notice that the $\sigma_R/\langle R\rangle=0.0$ data are the same as the $\sigma_\epsilon=0.0$ data discussed above and that $\sigma_R/\langle R\rangle\neq 0.0$ is just a different type of disorder from $\sigma_\epsilon\neq 0.0$ disorder. In the $\phi=90°$ plot of Fig. 4(b), curves are shown for $\sigma_R/\langle R\rangle=0.0$, 0.05, 0.1, 0.25, and 0.5. Here the mechanism for the $\theta=0°$ enhancement is the same as that given for the enhancement in Fig. 1(a), and the changes in $C^{(1)}$ with increasing σ_R arise from similar effects as those found in the systems with dielectric constant disorder.

Data for periodic on average systems are shown in Figs. 4(c) and 4(d). These present $C^{(1)}$ versus θ for $\phi=0°$ and $\phi=90°$, respectively. The four peaked structure in $C^{(1)}$ for $\phi=0°$ is only present for $\sigma_R/\langle R\rangle=0.0$ and 0.01. At higher disorders these features disappear and $C^{(1)}$ is relatively flat and featureless. Multiple scattering is important but contributes isotropically. In Fig. 4(d), the $C^{(1)}$ results at $\phi=90°$ increase in the neighborhood of $\theta=0°$ and 90° with increasing σ_R. For $\sigma_R/\langle R\rangle=0.25$ and 0.5 the peaks near $\theta=3°$ and 75° are shifted to $\theta=0°$ and 90°, respectively, and decreased in amplitude. This is due to the destruction of Bragg phase coherence due to the increasing difference (i.e., increasing σ_R) between the scattering particles.

A similar analysis to that presented in Sec. V A can be made for the dependence of the area under the unnormalized curves of $C^{(1)}$ on σ_R. This facilitates a discussion of the results for a variety of dielectric systems, having plots with similar topographical features. In Fig. 5 and Tables III and IV results of a linear regression to the form

$$A(\epsilon,\sigma_R)=A_0(\epsilon)+S(\epsilon)[\sigma_R/\langle R\rangle]^\gamma \tag{13}$$

are given for the homogeneously random system. (Note: To be brief, results for the periodic on average systems are omit-

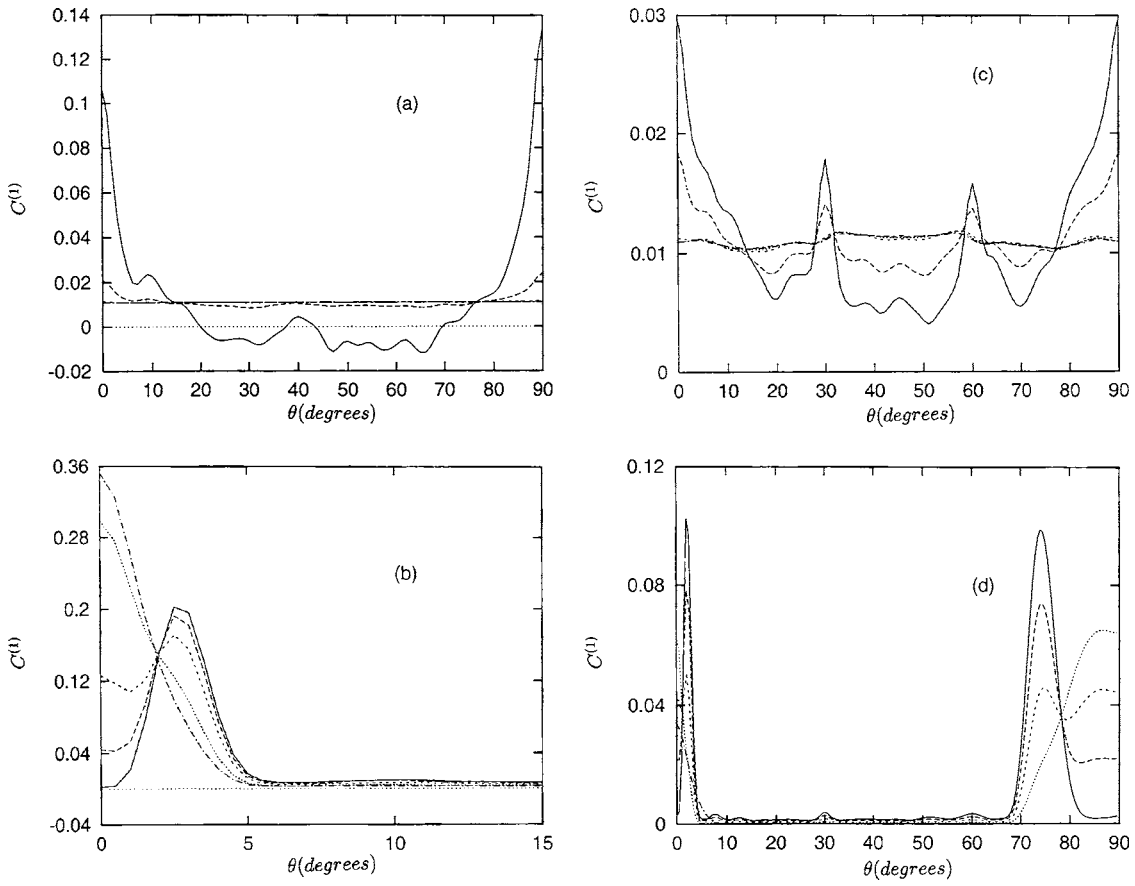

FIG. 4. Plots for the $\epsilon=-5$ homogeneously random system of the angular speckle correlation function along the $C^{(1)}$ envelope, scanned as a function of θ for (a) $\phi=0°$ with $\sigma_R/\langle R\rangle=0,0.01,0.05,0.10,0.5$, top to bottom on the left-hand edge, and (b) $\phi=90°$ with $\sigma_R/\langle R\rangle=0,0.05,0.10,0.25,0.5$, bottom to top on the left-hand edge. Plots for the periodic on average system of the angular speckle correlation functions along the $C^{(1)}$ envelope, scanned as a function of θ for (c) $\phi=0°$ with $\sigma_R/\langle R\rangle=0,0.01,0.05,0.10,0.25,0.50$, top to bottom on the left-hand edge, and (d) $\phi=90°$ with $\sigma_R/\langle R\rangle=0,0.05,0.10,0.25,0.50$, bottom to top on the right-hand edge.

ted.) In Eq. (13), $A(\epsilon,\sigma_R)$ is the area under the unnormalized curve, $A_0(\epsilon)=A(\epsilon,\sigma_r=0)$, and $S(\epsilon)$ and $\gamma(\epsilon)$ are fitting parameters determined from each of the ϵ data.

Figure 5 presents data for $\gamma(\epsilon)$ as a function of ϵ ranging between $\epsilon=-5$ and 5. The curve shows a gradual increase from $\gamma(\epsilon)\approx 1.5$ to $\gamma(\epsilon)\approx 2.0$ over this range. As with the homogeneous systems in Fig. 2, $\gamma(\epsilon)$ is greater for $\epsilon>0$ than for $\epsilon<0$. In general $\gamma(\epsilon)$ exhibits a mild form of universality in its dependence on ϵ.

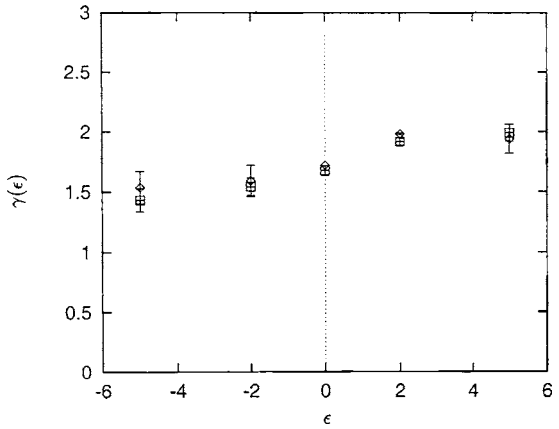

FIG. 5. A plot of $\gamma(\epsilon)$ versus ϵ for both $\phi=0°$ (diamonds) and $\phi=90°$ (squares) for $C^{(1)}$ in the homogeneous random system with statistically distributed radii.

Both Tables III and IV indicate a strong dependence of $A_0(\epsilon)$ and S on ϵ. For the $\phi=0°$ data, these quantities are largest at $\epsilon=\pm 5$ and decrease considerably in the range of ϵ between these upper and lower limiting values of ϵ. For the $\phi=90°$ data in Table IV, $A_0(\epsilon)$ as a function of ϵ exhibits peaks at $\epsilon=\pm 5$ and is smaller at ϵ between these limits. To a lesser degree this is also found in the data for S in Table IV. These variations in $A_0(\epsilon)$ and S are reasonable in that the scattering is more intense in systems with higher dielectric

TABLE IV. Random radii parameters $\ln S(\epsilon)$ and $A_0(\epsilon,\phi=90°)/A_0(\epsilon,\phi=0°)$ for $\phi=90°$.

Type	ϵ	$\ln S$	$A_0(\phi=90°)/A_0(\phi=0°)$
homogeneous $C^{(1)}$	−5	−2.43±0.20	52.57
homogeneous $C^{(1)}$	−2	−3.97±0.15	151.78
homogeneous $C^{(1)}$	0	−7.27±0.08	1064.24
homogeneous $C^{(1)}$	2	−5.78±0.06	800.59
homogeneous $C^{(1)}$	5	1.56±0.15	29.39

contrasts. One might expect the scattering fluctuations in such systems to be increased.

VI. KERR NONLINEAR MEDIA

In this section results are presented for a random spatial distribution of spheres having identical radii and Kerr nonlinear dielectric constants. The spheres in the simulation are of the same spatial distribution and sphere radii as those used to generate the data presented in Fig. 1. Now, however, the dielectric constant for the ith sphere of the array is given by $\epsilon_i=\epsilon+\lambda|\psi(\mathbf{r}_i)|^2$. Here ϵ is the linear part of the dielectric constant, λ is the Kerr parameter, and $\psi(\mathbf{r}_i)$ is the field wave function at the ith sphere. The parameters ϵ and λ are the same for each sphere so that the differences in the sphere dielectric constants arise from the difference in ψ at each sphere.

In the generation of data from the simulation an iterative approach is taken. To start with, for a given incident field $\psi_{inc}(\mathbf{r})$ and $\epsilon_i=\epsilon$ the $\psi(\mathbf{r}_i)$ at each dielectric sphere is computed. The results for $\psi(\mathbf{r}_i)$ are then used to compute the speckle correlation functions and new values of ϵ_i to be used in the following iteration. From $\psi_{inc}(\mathbf{r}_i)$ and the new ϵ_i the fields $\psi(\mathbf{r}_i)$ are again computed and used to obtain new ϵ_i for the next iteration. In terms of the sphere dielectric constants ϵ_i generated in a given iteration, the wave function $\psi(\mathbf{r}_i)$ at the spheres in the next iteration is given by

$$\psi(\mathbf{r}_k)=\sum_l\left[\tilde{1}-\tilde{M}\frac{\tilde{\epsilon}-1}{4\pi}\left(\frac{\omega}{c}\right)^2\right]^{-1}_{\mathbf{r}_k,\mathbf{r}_l}\psi_{inc}(\mathbf{r}_l), \qquad (14)$$

where $\tilde{\epsilon}=\epsilon_i\delta_{i,j}$. The system is treated in this fashion until convergence to a speckle correlation function is achieved.

In Fig. 6 results are presented for $C^{(1)}(\mathbf{q},\mathbf{k}|\mathbf{q}',\mathbf{k}')$ versus θ with $\phi=0°$ for a number of Kerr nonlinear systems. (Note: The areas under the curves in Fig. 6 have not been normalized to unity.) Figures 6(a) and 6(b) show plots with $\lambda|\psi_{inc}(\mathbf{r})|^2=0, \pm 0.1$ for $\epsilon=-5$ and 5, respectively. These give an indication, for typical values of ϵ, of the ϵ dependence of the Kerr nonlinear results. In particular, the difference between the $\lambda|\psi_{inc}(\mathbf{r})|^2=\pm 0.1$ data and the $\lambda=0$ data is a measure of the functional derivative of the speckle correlation functions with respect to $\epsilon(\mathbf{r})$. It is seen that the results for $\epsilon=-5$ are much less sensitive to the Kerr term than are those for $\epsilon=5$ and the effects of the sign of λ on the data are reversed in the two plots. For small Kerr nonlinearity the Kerr term generally shifts the correlation function plots along the vertical scale while retaining a similarity in general topographical features to the $\lambda=0$ curves. This is not surprising as the scattering in the system is approximately s wave. For much higher nonlinearities, however, this changes and the differences in the plots for increasing $\lambda|\psi|^2$ become much more complicated. In Fig. 6(c) $C^{(1)}$ versus θ for the $\epsilon=5$ system is studied for different $\lambda|\psi_{inc}(\mathbf{r})|^2=0, \pm 0.025$, and ± 0.1. A change in the general topographical features of the speckle correlation function is observed in the plots for $\lambda|\psi_{inc}(\mathbf{r})|^2=0.025$. This comes in part from the correlation in the dielectric changes between neighboring spheres that arises when the dielectric field on a given sphere of the system depends on the scattered fields it receives from its neighboring spheres. It indicates that, even for the small nonlinearities considered here, topographical changes can occur in the speckle correlation functions for changing intensities of the incident light.

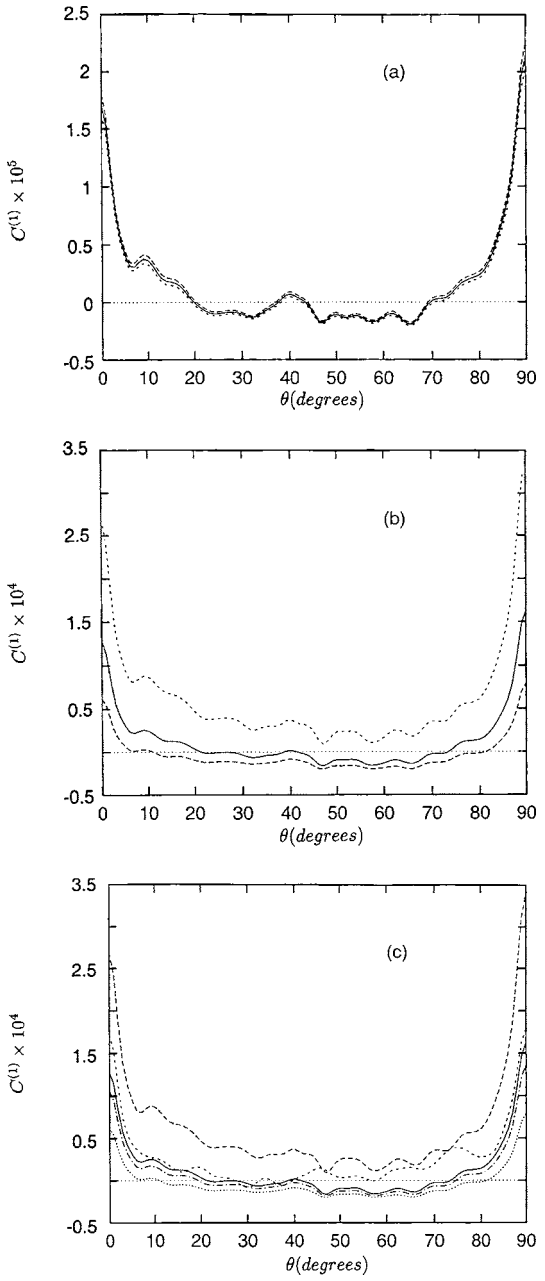

FIG. 6. Plots for the homogeneously random systems of the angular speckle correlation functions along the $C^{(1)}$ envelope, scanned as a function of θ for $\phi=0°$. The system is the same as those considered in Fig. 1 but instead of a Gaussian random distribution of dielectrics the dielectric constants of the spheres are given for the ith sphere by $\epsilon_i=\epsilon+\lambda|\psi(\mathbf{r}_i)|^2$. In (a) $\epsilon=-5$ and $\lambda|\psi_{inc}(\mathbf{r})|^2=0.1$ (bottom curve), =0 (middle curve), =−0.1 (upper curve); (b) $\epsilon=5$ and $\lambda|\psi_{inc}(\mathbf{r}_i)|^2=0.1$ (top curve), =0 (middle curve), =−0.1 (bottom curve); and (c) $\epsilon=5$ and $\lambda|\psi_{inc}(\mathbf{r})|^2=0.1$ (top curve), =0.025 (next lower curve), =0 (middle curve), =−0.025 (next lower curve), and =−0.1 (lowest curve).

VII. CONCLUSIONS

The sensitivity of $C^{(1)}$ and $C^{(10)}$ to the variances of the radii or dielectric constant distributions or Kerr term has been studied. Both homogeneous and periodic on average random distributions of the positions of the spheres were treated. It was found that (1) the correlation properties of systems of identical spheres are quite different from those in systems in which the spheres have an additional dielectric or radii disorder. (2) Multiple scattering effects are important and contribute with increasing dielectric or radii disorder in an isotropic manner in θ. Phase coherent same-path, time-reversed path, and Bragg scattering correlations are quickly overwhelmed by these isotropic contributions. (3) The θ-integrated intensity of $C^{(1)}$ and $C^{(10)}$ depend strongly on σ_ϵ and σ_R. These intensities scale with a power law dependence on σ_ϵ or σ_R, having critical exponents $\gamma(\epsilon)$ that depend weakly on the dielectric constant but exhibit universality with respect to the homogeneous or periodic on average nature of the system. This is an indication that the data have no scale (i.e., some fixed values of σ_ϵ or σ_R) that sets a change in behavior of the data as a function of dielectric or radii disorder. On the other hand, the θ-integrated intensity of the speckle correlation functions for $\sigma_\epsilon=\sigma_R=0$ strongly depend on the values of ϵ and ϕ. (4) The $C^{(1)}$ and $C^{(10)}$ contributions to the correlation functions for $\phi=0°$ and 90° exhibit different types of enhancements related to same-path and time-reversed path sequences phase-coherent processes. This is due to the fact that for $\phi=0°$ and 90° these functions sample different regions of wave vector space. Another consequence of this sampling difference is that the phase coherent processes are found to be overwhelmed at different rates between the $\phi=0°$ and 90° contributions to the speckle correlation functions. At points in wave vector space where the $\phi=0°$ and 90° plots merge, a peak is found in $\phi=90°$ data due to the difference in these two samplings. (5) In systems with Kerr nonlinearities, small intensity variations are found to shift the correlation functions along the vertical axes in plots of $C^{(1)}$ versus θ. In some cases a small variation in the field intensity causes topographical changes in the features of the correlation functions plotted as functions of θ. Small variations of field intensities can be used to study the functional derivatives of the correlation functions with respect to the ϵ.

The results presented confirm the possibility of using the angular speckle correlation functions to discern between media having the same average value but different variances of the dielectric constant distribution, or between random arrays of particles having the same average radius but different variances of the radii distribution. Not only do the magnitudes of the speckle correlation functions change, but the relative contributions of the $\phi=0°$ and 90° components change at different rates as well as some of the peaked features. This is of interest as recently measurements have been made of the speckle correlation functions from surface scattering[33,34] and it is hoped that our results would stimulate interest in similar measurements on the scattering from particulates. Such suggested applications of speckle for measurements on various biophysical systems and in engineering applications have been recently reviewed.[35,36]

As a final point we note that in this work the scalar wave theory was used. The scalar wave theory has been frequently applied in studies of the speckle correlations of scattered light and the Anderson localization of light in random media.[1,4–19,24–29] In many of these discussions the interest is in phase coherent processes and not on the polarization dependence of the scattering. The treatment is given for unpolarized incident light and, in addition, multiple scattering of light in a random medium tends to average the polarization so that the scalar wave theory should be acceptable. For the scattering in highly symmetric and periodic systems such averaging is not present so that the scalar wave theory is less acceptable. In our system of spheres a problem is the scattering from the $\epsilon=-2$ system.[37] In the complete vector treatment the long wavelength scattering cross section from a dielectric sphere diverges at $\epsilon=-2$ due to the excitation of a polariton in the sphere. (This divergence is not present in the scalar wave treatment.) The divergence is an artifact of the induced polarization of a dielectric sphere in a uniform external field and comes from the spherical geometry. It is a problem with the vector treatment and must itself be resolved in the application of the vector theory. A resolution of this problem in the vector treatment and in our model is to realize that in a real particulate system the particles will not all be spheres and this will tend to reduce the effect.[37] In addition, there will be accompanying nonlinearities and dielectric losses that will limit the resonance. A possible way to handle some of these types of effects in the scalar wave theory is by treating the dielectric constant in the scalar wave model as an effective dielectric constant or to realize that the correlation effects of unpolarized incident light that we are studying are averaged by the multiple scattering between spheres and the fact that the correlation functions are those for the total scattered energy current. The results from our model should in any case give a reasonable representation of the phase coherent properties and the relative intensities of the various different wave vector samplings in the $C^{(1)}$ and $C^{(10)}$ contributions to the speckle correlation functions. Other simulation methodologies (e.g., the coupled dipole method,[38,39] finite-difference time-domain methods,[40] and finite element methods[41]) that treat the vector nature of light could find possible applications to our system. The scalar wave treatment, however, has been extensively used as a basis for the study of speckle correlation functions and, as has been pointed out by Feng,[24] is a good general treatment that handles the phase coherent multiple scattering of light, acoustical, and scalar electron waves by a general random media. It thus lends itself to a dual purpose.

Finally, we emphasize that our formal solution in Eq. (8) for the scattering from the system of spheres is the **T**-matrix formulation of scattering. [A form of Eq. (8) was originally used in discussions of speckle in Phys. Rev. B **64**, 165204 (2001) that are related to those given in this paper.] The **T**-matrix formulation is a common formulation that is found in most textbooks and used in most papers that treat all multiple scattering from random systems. The off-diagonal components of $\tilde{M}$ in Eq. (8) are responsible for the multiple scattering between the spheres. In addition, the scalar wave theory has been commonly used in many recent discussions

of speckle correlations of unpolarized incident light such as in Ref. 1 and most of the other recent papers referred to in this paper. This is due to the origin of speckle in phase coherent properties, the tendency to average over polarizations of light in the scattering by random media, and the definition of the correlation function in terms of total field intensities. The scalar wave theory does not limit the multiple scattering between the spheres in the system and is of interest itself as it is applicable to a variety of nonoptical scattering problems. Some comparisons of the scalar wave treatment with experiments have also been favorably made.[6,12,13,15,16,24,27,29]

APPENDIX: SCALING

We used the fit $A(\epsilon,\sigma_\epsilon)-A_0(\epsilon)=S(\epsilon)\sigma_\epsilon^\gamma$ based on the theory of scaling and critical exponents in statistical physics. In our treatment γ is a critical exponent.

Scaling theory is based on the observation that about points in phase space at which a system undergoes changes of state, the properties of the system often exhibit power law forms in their dependence on the variables driving the change of state.[42–46] The systems in question can be quite general statistical systems;[42–48] e.g., thermodynamics, random geometric, nonlinear dynamical, animal and chemical populations, scattering from disordered media, etc. General references for a detailed treatment are Refs. 42 and 46–48.

To understand our application, let us argue by analogy with magnetic systems. First consider the ferromagnetic transition. Below and near the critical temperature, T_c, it is well known that the magnetization as a function of temperature, $M(T)$, obeys the relation $M(T)=M_0[(T_c-T)/T_c]^\beta$. Here β is the critical exponent. It is found in some cases to exhibit certain universality properties, i.e., it only depends on properties such as lattice or spin dimensionality and is independent of other details of the system such as the strengths of the exchange interactions or whether the lattice is a bcc or fcc lattice. There are other critical exponents, however, in some magnetic system that can depend on the details of the interactions and are in this sense not universal.

In our scattering systems the speckle correlation function and its integrated envelope exhibit a type of state transition. If the media formed by the spheres were perfectly periodic or perfectly uniform, then the system would exhibit only Bragg diffraction or a refractive index, respectively. Whichever of these two occurs depends on the wavelength of the light. The introduction of positional disorder, dielectric disorder, and/or radii disorder drives the system to exhibit diffuse scattering. Each of these three types of disorder are characterized by its own set of parameters measuring the degree of the disorder. Each set of parameters can independently drive the diffuse scattering. The speckle correlation functions we study are computed for the diffuse scattering and become zero in the absence of disorder. (This is similar to the magnetization which disappears at T_c.) Consequently, power law behavior should be observed in the disorder parameters determining the speckle correlation functions in our system. The object in this paper is to determine the power law dependence of the speckle correlation functions on the various disorder parameters, the critical exponents, and the universality properties of the critical exponents. Another important aspect of the power law dependence of the speckle correlation function on the disorder parameters is that it indicates the absence of a natural scale that determines how the system depends on the disorder variables.

[1] A. R. McGurn and A. A. Maradudin, Phys. Rev. B **64**, 165204 (2001).
[2] M. Nieto-Vesperinas, *Scattering and Diffraction in Physical Optics* (Wiley, New York, 1991).
[3] J. D. Jackson, *Classical Electrodynamics*, 3rd ed. (Wiley, New York, 1998).
[4] B. Shapiro, Phys. Rev. Lett. **57**, 2168 (1986).
[5] S. Feng, C. Kane, P. A. Lee, and A. D. Stone, Phys. Rev. Lett. **61**, 834 (1988).
[6] I. Freund, M. Rosenbluh, and S. Feng, Phys. Rev. Lett. **61**, 2328 (1988).
[7] R. Berkovits, M. Kaveh, and S. Feng, Phys. Rev. B **40**, 737 (1993).
[8] R. Berkovits and M. Kaveh, Phys. Rev. B **41**, 2635 (1990).
[9] L. Wang and S. Feng, Phys. Rev. B **40**, 8284 (1989).
[10] R. Berkovits, Phys. Rev. B **42**, 10750 (1990).
[11] A. R. McGurn and A. A. Maradudin, Phys. Rev. B **39**, 13160 (1989).
[12] N. Garcia and A. Z. Genack, Phys. Rev. Lett. **63**, 1678 (1989).
[13] M. P. van Albada, J. F. de Boer, and A. Lagendijk, Phys. Rev. Lett. **64**, 2787 (1990).
[14] *Scattering and Localization in Random Media*, edited by P. Sheng (World Scientific, Singapore, 1990).
[15] M. J. Stephen and G. Cwilich, Phys. Rev. B **34**, 7564 (1986).
[16] M. J. Stephen and G. Cwilich, Phys. Rev. Lett. **59**, 285 (1987).
[17] A. Lagendijk and B. A. van Tiggelen, Phys. Rep. **270**, 143 (1996).
[18] D. A. Wiersma, P. Bartolini, A. Lagendijk, and R. Righini, Nature (London) **390**, 671 (1997).
[19] Y. Imry, *Introduction to Mesoscopic Physics* (Oxford University Press, New York, 1997).
[20] V. Malyshkin, A. R. McGurn, T. A. Leskova, A. A. Maradudin, and M. Nieto-Vesperinas, Opt. Lett. **22**, 946 (1997).
[21] V. Malyshkin, A. R. McGurn, T. A. Leskova, A. A. Maradudin, and M. Nieto-Vesperinas, Waves Random Media **7**, 479 (1997).
[22] B. Danila and A. R. McGurn, Phys. Rev. B **71**, 115421 (2005).
[23] V. Malyshkin, A. R. McGurn, and A. A. Maradudin, Phys. Rev. B **59**, 6167 (1999).
[24] S. Feng, in *Scattering and Localization of Classical Waves in Random Media*, edited by P. Sheng (World Scientific, Singapore, 1990).
[25] S. E. Skipetrov and R. Maynard, Phys. Rev. B **62**, 886 (2000).
[26] S. E. Skipetrov, Phys. Rev. Lett. **93**, 233901 (2004).
[27] A. A. Chabanov, B. Hu, and A. Z. Genack, Phys. Rev. Lett. **93**, 123901 (2004).
[28] P. Sebbah, B. Hu, A. Z. Genack, R. Pnini, and B. Shapiro, Phys.

Rev. Lett. **88**, 123901 (2002).
[29] P. Lodahl and A. Lagendijk, Phys. Rev. Lett. **94**, 153905 (2005).
[30] D. J. Griffiths, *Introduction to Quantum Mechanics* (Prentice-Hall, Englewood Cliffs, NJ, 1995), Chap. 11.
[31] A. Messiah, *Quantum Mechanics*, Vol. II (North-Holland, Amsterdam, 1966).
[32] R. D. Mattuck, *A Guide to Feynman Diagrams in the Many-Body Problem* (McGraw-Hill, New York, 1976).
[33] Z.-H. Gu and A. R. McGurn, Proc. SPIE **3784**, 285 (1999).
[34] C. S. West and K. A. O'Donnell, Phys. Rev. B **59**, 2393 (1999).
[35] Y. Aizu and T. Asakura, in *Trends in Optics: Research, Development, and Applications*, edited by A. Consortini (Academic, San Diego, 1996), p. 27.
[36] R. S. Sirohi, in *International Trends in Optics and Photonics*, edited by T. Asakura (Springer, Berlin, 1999), p. 318.
[37] D. J. Berman and D. Stroud, in *Solid State Physics*, Vol. 46, edited by H. Ehrenreich and D. Turnbull (Academic, Boston, 1992), pp. 148–269.
[38] E. M. Purcell and C. R. Pennypacker, Astrophys. J. **186**, 705 (1973).
[39] P. C. Chaumet, A. Rahmani, F. de Fornel, and J.-P. Dufour, Phys. Rev. B **58**, 2310 (1998).
[40] A. Taflove, *Computational Electrodynamics: The Finite-Difference Time-Domain Method* (Artech House, Norwood, 1995).
[41] L. R. Ram-Mohan, *Finite Element and Boundary Element Applications in Quantum Mechanics* (Oxford University Press, New York, 2002).
[42] R. K. Pathria, *Statistical Mechanics*, 2nd ed. (Butterworth-Heinemann, Oxford, 2001), Chaps. 11–13.
[43] N. Goldenfeld, *Lectures on Phase Transitions and the Renormalization Group* (Addison-Wesley, Reading, MA, 1992).
[44] G. Toulouse, *Introduction to the Renormalization Group and to Critical Phenomena* (Wiley, London, 1977).
[45] R. J. Creswick, H. A. Farach, and C. P. Poole, Jr., *Introduction to Renormalization Group Methods in Physics* (Wiley, New York, 1992).
[46] P. M. Chaikin and T. C. Lubensky, *Principles of Condensed Matter Physics* (Cambridge University Press, New York, 2000).
[47] M. R. Schroeder, *Fractals, Chaos, Power Laws: Minutes from an Infinite Paradise* (Freeman, New York, 1991).
[48] D. Sornette, *Critical Phenomena in Natural Sciences* (Springer, Berlin, 2000).